Astron. Astrophys. 211, 173–186 (1989)

ASTRONOMY AND ASTROPHYSICS

Rotational modulation and flares on RS Canum Venaticorum and BY Draconis stars

X. The 1981 October 3 flare on V711 Tauri (= HR 1099)⋆

J.L. Linsky[1,⋆⋆,⋆⋆⋆], J.E. Neff[1], A. Brown[1], B.D. Gross[1], T. Simon[2,⋆⋆], A.D. Andrews[3,⋆⋆], M. Rodonò[4,⋆⋆], and P.A. Feldman[5]

[1] Joint Institute for Laboratory Astrophysics, National Bureau of Standards and University of Colorado, Boulder, CO 80309-0440, USA
[2] Institute of Astronomy, University of Hawaii, Honolulu, HI 96822, USA
[3] Armagh Observatory, Armagh, BT61 9DG, Northern Ireland
[4] Institute of Astronomy, University of Catania and Astrophysical Observatory, I-95125 Catania, Italy
[5] Herzberg Institute of Astrophysics, NRC of Canada, Ottawa, ON K1A OR6, Canada

Received March 9, accepted June 22, 1988

Summary. We present a unique set of *high resolution* spectra of V711 Tauri = HR 1099 (G5 V + K1 IV) obtained with both the SWP and LWR cameras of IUE, together with simultaneous 6.4 GHz microwave emission and optical photometry, during a bright flare on 3 October 1981. The electron density of the flaring plasma at $6\,10^4$ K was about $1\,10^{11}$ cm^{-3}, 15 times higher than quiescent, and the radiating volume was about $2\,10^{30}$ cm^3, 200 times smaller than quiescent. A constrained multigaussian fit to the Mg II k line profile shows that the flare component profile was very broad (66 km s^{-1} FWHM), indicating significant turbulence, and redshifted by 90 ± 30 km s^{-1} relative to the center of mass of the K 1 IV star. We interpret this redshift as due to downflowing material probably located above a large starspot known from optical photometry and Doppler imaging to be near disk center of the K 1 IV star during the flare. The flux of kinetic energy at flare peak due to the downflow and turbulence was $\leq 1\,10^{32}$ erg s^{-1}, essentially equal to the flare radiative luminosity. The microwave emission was probably gyrosynchrotron emission from mildly relativistic electrons (typical energy 1.7 MeV) trapped in magnetic flux tubes emerging from the whole area of this spot.

Key words: stars: atmospheres of – stars: binaries, spectroscopic – stars: chromospheres of – stars: flare – stars: V711 Tau – stars: radio radiation of

Send offprint requests to: J.L. Linsky

⋆ Based on observations collected with IUE at the ESA satellite Tracking Station, Villafranca (Madrid, Spain) and at NASA Goddard Space Flight Center (Greenbelt, MD, USA).
⋆⋆ Guest observer, International Ultraviolet Explorer (IUE).
⋆⋆⋆ Staff Member, Quantum Physics Division, National Bureau of Standards.

1. Introduction

As originally defined by Hall (1976), RS CVn-type systems consist of detached binaries with an F or G-type component of luminosity class V or IV, and typically a cooler early K-type secondary of luminosity class IV. The orbital periods are 1–14 days, and strong Ca II H and K emission is typically observed from one or both stars. Many observers have studied the rich phenomenology of these systems at wavelengths from X-rays to the radio. These phenomena are reminiscent of what is observed on the Sun, but they are vastly more energetic and often cover a much larger area of the stellar surface. Recent reviews include those of Rodonò (1983), Bopp (1983), and Linsky (1983).

In earlier papers of this series we have presented results from using the IUE satellite and coordinated optical, radio, and X-ray observations to study the surface brightness distribution and phase-dependent ultraviolet spectra of important members of the RS CVn class. In this paper we will study a flare on V711 Tau that occurred during the October 1981 monitoring program described in previous papers in the series.

Extremely energetic and long-lived flares are often detected from RS CVn systems at radio, optical, ultraviolet, and X-ray wavelengths. A particularly well-studied event is the February 1978 flare on V711 Tau described in a series of papers in the December 1978 issue of the *Astronomical Journal*.

The extensive set of microwave observations of RS CVn flares, many of which persist for days with flux levels as large as 1 Jy, have been summarized by Gibson (1980, 1981), Hjellming and Gibson (1980), Feldman (1980, 1983), and Mullan (1985). Unlike flares on M dwarfs, RS CVn flares are rarely detected in broadband optical photometry (Patkos, 1981), because of the bright photospheric continuum of the G and K-type stars against which they must be measured. On the other hand, enhanced Hα emission is a good indicator of flares in RS CVn systems (Bopp, 1983; Fraquelli, 1982, 1984; Catalano, 1986), and the time history of the Hα equivalent width during flares is well correlated with the microwave flux.

Flares have been detected with *Copernicus* and with IUE as enhanced ultraviolet emission line fluxes in several systems including V711 Tauri (Weiler et al., 1978), UX Arietis (Simon et al., 1980), λ Andromedae (Baliunas et al., 1984), IM Pegasi (Buzasi et al., 1987), and AY Ceti (Simon and Sonneborn, 1987). High-resolution ultraviolet spectra are extremely important in studies of RS CVn flares, because they can help answer two basic questions: (1) the volume and location of the 10^4–10^5 K flaring plasma, and (2) the nature of mass motions within the flaring plasma.

The nature of the mass motions during flares can be inferred from the observed asymmetric or very broad line profiles. Bopp (1983) has summarized the diverse shapes of Hα profiles observed during flares, which range from simple increases in brightness with no additional broadening (Fraquelli, 1984) to symmetric broad profiles with total width of 400 km s^{-1} (Furenlid and Young, 1978) to the very broad Hα profile observed during the August-September 1978 flaring episode on SZ Psc suggestive of a mass transfer event (Bopp, 1981). High-resolution Mg II emission line profiles (Simon et al., 1980) observed during the 1 January 1979 flare on UX Ari exhibited broad wings extending 475 km s^{-1} to the red but no enhancement of the blue wings. The authors attributed the red-shifted line wings to material impacting the G star at the free-fall velocity, and they speculated that large magnetic structures attached to both stars might occasionally interact and interconnect (see Uchida and Sakurai, 1983). The only other high-resolution flare spectra published to date are the five long-wavelength spectra of the 5–6 November 1982 λ And flare (Baliunas et al., 1984), which show a small enhancement only on the red wing of the Mg II lines.

Here we report on the 3 October 1981 flare on V711 Tau; a unique event in that both short- and long-wavelength high-resolution spectra were obtained, together with coordinated optical photometry and 6424 MHz observations. We describe in Sect. 2 the observations, their analysis, and the probable location of the flare. We then discuss in Sect. 3 the physical properties of this flare and compare it to flares in other RS CVn systems and the Sun. Linsky et al. (1986) discussed the data set in a preliminary way.

2. IUE observations of the 3 October 1981 flare on V711 Tau

2.1. The IUE observing program

We observed V711 Tau (=HR 1099 = HD 22468) during 2–7 October 1981 to study modulation of the emission from inhomogeneous surface structures over the 2.84-day orbital (and rotational) period of the system. The observations were interleaved within a larger program of rotational modulation studies of II Peg, AR Lac, and BY Dra, for which we combined IUE observing time obtained under collaborative NASA, ESA, and SERC programs. The larger observing program is described in Paper III (Rodonò et al., 1987), and the coordinated photometry is described in Paper I (Rodonò et al., 1986). We summarize in Table 1 the parameters for the IUE spectra that were obtained immediately before, during, and immediately after the flare event on V711 Tau. Table 2 contains a summary of the flare parameters that will be derived in this paper. The complete log of IUE spectra is given in Table 2 of Paper III.

When the low dispersion image SWP 15161-LO (mid exposure time 0512 UT on 3 October 1981) was read down from the satellite, the obviously enhanced line fluxes indicated a major flare event on V711 Tau. A subsequent call to the Algonquin Radio Observatory confirmed this, as the 6424 MHz microwave flux was then about 160 mJy, compared with quiescent levels of less than 50 mJy. By that time the IUE satellite had already maneuvered to and was observing the next target in our program. We immediately returned to V711 Tau to obtain two spectra near the peak of the flare (SWP 15161-LO and LWR 11668-HI) and four spectra obtained 5–8 hours later during the decay phase (LWR 11670-HI, SWP 15163-HI, LWR 11671-HI, and SWP 15164-LO).

2.2. Integrated emission line fluxes

The reduction and analysis of the SWP spectra are described in Paper III. The absolute flux scale for IUE is considered to be accurate to 10% (cf. Bohlin, 1986), and the 1σ scatter for optimally-exposed 5 Å wide continuum bands (roughly equivalent to an emission line in low dispersion) is 5% (Bohlin and Grillmair, 1987).

Table 1. IUE observations of V711 Tau = HR 1099 during the 1981 October 3 flare

IUE	Image[a]	UT (mid. exp.)	Orbital phase[b]	Exposure time (min)	FES magnitude	Comments
LWR	11665-HI	2111[c]	0.066	15	5.85	Preflare
SWP	15158-LO	2203[c]	0.078	45	–	Preflare
SWP	15161-LO	0512	0.183	35	5.81	Flare peak?
LWR	11668-HI	0635	0.204	15	5.77	Flare peak?
LWR	11670-HI	1047	0.265	15	5.85	Flare
SWP	15163-HI	1208	0.285	120	–	Flare
LWR	11671-HI	1322	0.303	15	5.84	Flare
SWP	15164-LO	1349	0.310	15	5.88	Flare
LWR	11674-HI	2136	0.424	15	5.91	Postflare
SWP	15167-LO	2155	0.429	25	–	Postflare

[a] Suffix: LO = low dispersion, HI = high dispersion.
[b] Orbital phases at mid-exposure from JD(hel.) 2442766.080 + 2.83774 E, where zero phase corresponds to conjunction with the K star in front (Fekel, 1983; Paper I).
[c] Previous day, 1981 October 2.

Table 2. Summary of flare parameters

Date of the flare	1981 October 3
Time of the flare peak	before 0512 UT
Phase of the flare peak	before 0.183
Emission line flux ratios (flare/preflare)	
– for transition region lines	2.4
– for chromospheric lines	1.5
Flare peak luminosities	
– all measured UV lines ($\Delta L_{\rm flare}$)	$0.132\,10^{32}$ erg s^{-1}
– all radiation for $4.0 \lesssim \log T_e \leq 5.3$ ($\Delta L_{\rm rad}$)	1.2–$1.7\,10^{32}$ erg s^{-1}
– possible visual flux enhancement (ΔL_v)	$1.4\,10^{32}$ erg s^{-1} (?)
Kinetic energy flux ($f_{\rm KE}$)	$\leq 1\,10^{32}$ erg s^{-1}
Flare decay timescale	
– for microwave emission	$\sim 2^{\rm h}$
– for transition region lines	$\sim 5^{\rm h}$
– for chromospheric lines	$\sim 12^{\rm h}$
Total radiated energy for $4.0 \lesssim \log T_e \lesssim 5.3$	$2.4\,10^{36}$ erg
$v \sin i$[a]	38 km s^{-1}
Δv (flare − K1 IV star) in Mg II k	90 ± 30 km s^{-1}
FWHM of flare Mg II k component	66 km s^{-1}
Most probable rms speed for flare Mg II k component	49 km s^{-1}
N_e (at $6\,10^4$ K) at flare peak	$\approx 1\,10^{11}$ cm^{-3}
Flare peak volume (at $6\,10^4$ K)	8–$36\,10^{29}$ cm^3
Flare peak loop footpoint separation	4.1–$6.5\,10^{10}$ cm
Starspot area (18% of visible surface)[a]	$4.3\,10^{22}$ cm^2
Peak 6424 MHz flux	170 mJy
T_B (6424 MHz) of flare peak	$\lesssim 2\,10^{10}$ K
Flare surface area at peak	
– 6424 MHz radiation	$\approx 6\,10^{22}$ cm^2
– UV emission lines (at $6\,10^4$ K)	$1.2\,10^{21}$ cm^2

[a] Not derived in this study but assumed from earlier work

Random flux errors for weaker lines can be much larger. The variation with phase of the integrated line fluxes and the visual magnitudes are shown in Fig. 3 of Paper III. We summarize in Table 3 here the integrated emission line fluxes at Earth measured from the spectra obtained immediately prior to the flare (images LWR 11665-HI and SWP 15158-LO) and at what we call the "flare peak" (SWP 15161-LO and LWR 11668-HI). We have no way of knowing the true maximum fluxes at the peak of the flare, only the flux averaged over the 35 or 120 min exposure times. Therefore, the "flare peak" fluxes are lower limits to the true maximum fluxes during the flare. The "flare peak" spectrum is compared with the mean quiescent spectrum in Fig. 2 of Paper III. Table 3 summarizes the enhancements in flux (flare peak minus preflare), the ratios of the flare peak to the preflare flux, and the luminosities of the flare (flare peak minus preflare) for each line, assuming a distance of 31 pc (Paper III) and negligible interstellar absorption. Our method for estimating the intrinsic Lα flux is described below.

We call attention to the following significant aspects of these data.

(1) The well-exposed transition region lines (e.g. C IV, Si IV, and C II) strengthen by a factor of about 2.4 (except the density-sensitive C III] 1909 Å line), whereas the chromospheric lines (e.g. Mg II, Si II, O I, and C I) strengthen by about a factor of 1.5. Table 4 summarizes the corresponding enhancement factors for flares on UX Ari, λ And, AY Cet, and IM Peg. During all of these flares the fluxes of the transition region lines increased by significantly larger factors than the chromospheric lines, with the most luminous flare (UX Ari) having the largest enhancement factors.

(2) The ultraviolet continuum, especially the 1580–1630 Å region (see Table 3), also brightened during the flare, as previously noted by Baliunas et al. for the λ And flare and by Buzasi et al. for the IM Peg flare.

(3) The Lα and Mg II lines dominate the radiative fluxes for the observed ultraviolet lines in Table 3, as previously noted for the UX Ari, λ And, and AY Cet flares. However, several spectral features that could be important in the energy budget for material in the $4\,10^3$ to $2\,10^5$ K temperature range are omitted from Table 3. For example, Hα usually brightens during flares (e.g. Bopp, 1983), but we have no simultaneous observations of this line. Many weak Fe II lines in the 2300–2800 Å spectral region brightened during the UX Ari flare, but we measured no significant increase in the emission from the six brightest Fe II lines in the flare peak spectrum.

2.3. *Emission line profiles*

The Mg II h and k line profiles at the ten observed orbital phases were analyzed at the Colorado Regional Data Analysis Facility by fitting the spectral lines with one to five gaussian profiles as

Table 3. V711 Tau fluxes before and near the peak of the 1981 October 3 flare

Spectral feature	Flux at Earth (10^{-12} erg cm^{-2} s^{-1})			Ratio (flare/preflare)	ΔL^{c}_{flare} (10^{30} erg s^{-1})
	Preflare[a]	Flare peak[b]	Enhancement		
N v 1240 Å	0.5	2.5	2.0	5.0	0.23
C iv 1550 Å	4.5	12.1	7.6	2.7	0.87
Si iv 1400 Å	1.4	3.4	2.0	2.4	0.23
Al iii 1860 Å	0.32	0.79	0.47	2.5	0.05
C iii 1175 Å	1.3	3.4	2.1	2.6	0.24
C iii 1909 Å	0.43	0.48	0.05	1.1	0.01
Si iii 1892 Å	0.45	1.1	0.67	2.5	0.08
O iii 1666 Å[d]	0.36	0.75	0.39	2.1	0.04
C ii 1335 Å	3.4	7.0	3.6	2.1	0.41
Si ii 1812Å	1.7	2.8	1.1	1.6	0.13
O i 1304 Å	2.0	4.0	2.0	2.0	0.23
C i 1561 Å	0.21	0.23	0.02	1.1	0.00
C i 1657 Å	1.5	1.6	0.1	1.1	0.01
Mg ii k (2796 Å)	29.3	42.0	12.7	1.4	1.46
Mg ii h (2803 Å)	22.7	31.0	8.3	1.4	0.95
He ii 1640 Å	1.9	2.9	1.0	1.5	0.12
Sum	72.	116.	44.		5.1
Lα[e]	116.	186.	70.	1.6	8.1
Sum (with Lα)	188.	302.	114.		13.2
1580–1630 Å	0.87	1.54	0.67	1.8	0.078
1750–1780 Å	1.12	1.51	0.39	1.3	0.045

[a] From images LWR 11665-HI (phase 0.066) and SWP 15158-LO (phase 0.078).
[b] From images SWP 15161-LO (phase 0.183) and LWR 11668-HI (phase 0.204).
[c] Luminosity of the flare only (flare peak minus preflare) assuming a distance of 31 pc and no interstellar absorption.
[d] Include Al ii and Fe ii blends.
[e] Comparison for V711 Tau Lα flux was obtained from the nonflare spectrum SWP 9571-HI at a similar phase. Fluxes given are estimates of the intrinsic stellar Lα emission (see discussion in text).

Table 4. Enhancement factors for emission line fluxes during flares

	V711 Tau 1981 Oct 3	UX Ari 1979 Jan 1	λ And 1982 Nov 6	AY Cet 1983 Dec 6	IM Peg 1985 July 5
Transition region lines (C iv, Si iv, C ii)	2.4	5.5	3.0	3.0	4.2
Chromospheric lines (Mg ii, Si ii, O i, C i)	1.5	2.5	1.2	1.3	1.8

described in Paper III and by Walter et al. (1987b, Paper IV). The fitting program (Neff, 1987) is based upon the CURFIT program (Bevington, 1969), which uses the Marquardt algorithm to minimize the chi-square of the fit. The Mg ii k line profiles were fitted with two broad symmetric emission components centered close to the radial velocities of the K and G stars, a narrow absorption feature that we ascribe to interstellar absorption and use as a wavelength fiducial, and one or two additional gaussian components. (See Fig. 1)

The width of the interstellar feature (i.e., the instrumental resolution) and the radial velocities of the two stars are known a priori. The position and equivalent width of the interstellar feature must remain constant. Applying these constraints, we constructed a series of multi-gaussian fits to the observed line profiles (see Paper III). These fits showed that the line width and flux of each stellar component are roughly constant, apart from the flare. We also found that a small additional gaussian component (hereafter called component P) was frequently required to match the excess emission in the line wings, but we were unable to determine whether this emission was due to discrete regions in the stellar system (e.g., plages) or due to the intrinsic shape of the stellar line profiles that cannot be described by simple

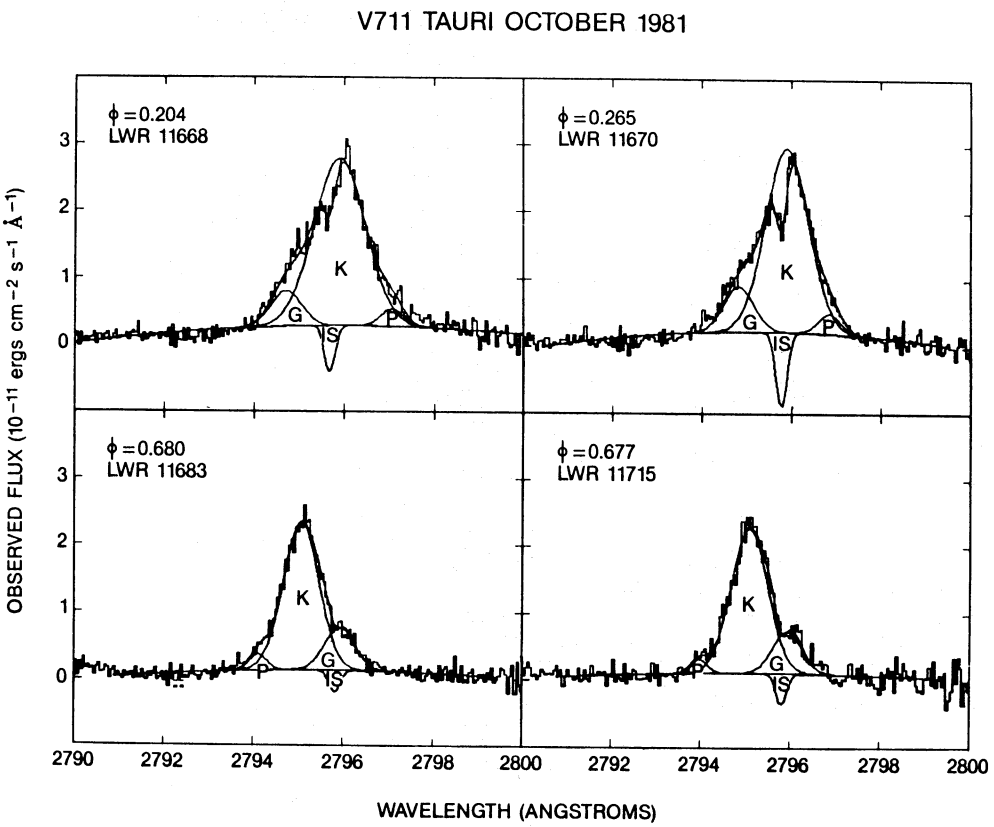

Fig. 1. Observed Mg II k line profiles and four gaussian fits to these profiles for two flare spectra (phases 0.204 and 0.265) and two quiescent spectra near the opposite quadrature (phases 0.680 and 0.677). The gaussian profiles are identified with the K1 IV star (K), G5 V star (G), a plage (P), and Mg II interstellar absorption (IS)

gaussians. The resulting wavelengths, integrated fluxes, and FWHM of the gaussian components (corrected for the 30 km s^{-1} instrumental profile) are summarized in Table 5.

In Fig. 1 we show Mg II k line profiles obtained during the flare (phases 0.204 and 0.265) and profiles obtained at nearly opposite phases (0.680 and 0.677) 1.3 and 4.2 days later, when the radial velocities of the K and G stars are reversed and the emission had decayed to its quiescent level. Also shown are the gaussian decompositions. The increase in the flux in the K star component during the flare is pronounced, while the flux in the G star gaussian component is nearly unchanged. This is more clearly seen in Fig. 2, which shows the variation with phase (and thus time) of the integrated Mg II k line flux for each star. The centroid velocity of the brighter Mg II gaussian (labelled K) during the flare is 15 $\pm$ 5 km s^{-1} relative to the predicted radial velocity of the K star. The absence of an additional component to the line profile and the small width increase and net red shift of the single gaussian indicates that the flaring plasma was moving away from the observer (either due to its location near the receding limb of the K star or to downflow or to a combination of the two causes) with a broad intrinsic profile.

Additional evidence that the flare occurred on or near the K star is shown in Fig. 3, where we plot the observed Mg II k line profiles at flare peak (phase 0.204) and 7 hours later at phase 0.303. Shifts in the wavelength scale in this time period are expected to be small, and the radial velocities of each star are the same at these two phases, which are symmetric about quadrature. We note that the *only* difference between the profiles is to the right of peak flux at radial velocities corresponding to the K star, thus strengthening our conclusion that the flare occurred on or near the K star.

In Fig. 4 we show the flare peak (phase 0.204) Mg II k line profile and a different four-gaussian fit in which the integrated fluxes and widths of three of the gaussians were constrained to the mean quiescent values for the G star, K star, and interstellar medium. The radial velocities for the three gaussians were also fixed to the values appropriate for this phase. The residual emission was then modelled with a fourth gaussian component to represent the flare alone. The resulting fit to the observed profile is comparable in quality to the unconstrained four-gaussian fit shown in Fig. 1. This constrained modelling procedure retains the flux, width and radial velocity of the mean global quiescent emission of the K star, which we believe should still be present while a portion of the K star flares. The flare gaussian component is centered at 90 $\pm$ 30 km s^{-1} with respect to the center of mass of the K star. This Doppler shift indicates emission from material for which the sum of the projected rotational and intrinsic flow velocities is about 90 km s^{-1}. The integrated k-line flux in the flare component alone is 8.2 10^{-12} erg cm^{-2} s^{-1} at Earth, similar to the flare enhancement determined previously. The FWHM of the flare component, corrected for instrumental broadening, is 66 km s^{-1}.

As shown in Fig. 1, we initially included an additional component (marked P) in the line wing. Some or all of this emission is probably due to the flare. Unfortunately, we cannot precisely determine the non-flaring shape of the line wing at this phase

Table 5. Parameters for the multigaussian fits to the Mg II k line profiles

Image	Orbital phase	Wavelength – 2790 Å				Integrated flux (10^{-12} erg cm^{-2} s^{-1})			Deconvolved[a] FWHM (km s^{-1})		
		Interstellar	K Star	G Star	*P*	K Star	G Star	*P*	K Star	G Star	*P*
LWR 11660-HI	0.916	5.69	5.19	5.58	–	24.2	5.1	–	74	45	–
LWR 11665-HI	0.066	5.73	5.62	5.09	6.69	23.1	4.8	1.5	55	45	23
LWR 11668-HI	0.204	5.67	5.89	4.70	7.05	35.8	4.6	1.6	85[c]	49	32
LWR 11670-HI	0.265	5.74	5.87	4.78	6.82	33.1	5.7	1.9	70	47	33
LWR 11671-HI	0.303	5.73	5.86	4.78	7.00	31.9	5.7	1.1	70	49	32
LWR 11674-HI	0.424	5.79	5.73	5.09	6.78	22.8	4.7	0.9	58	44	23
LWR 11679-HI	0.557	5.73	5.31	5.56	4.36	24.8	3.5	1.1	68	49	22
LWR 11683-HI	0.680	5.80	5.04	5.91	4.10	22.1	5.4	1.2	58	47	22
LWR 11691-HI	0.005	5.79	5.57	5.42	6.57	25.1	5.0	1.6	56	46	22
LWR 11715-HI	0.677	5.78	5.06	5.91	3.94	21.2	5.1	1.0	59	46	22
SWP 15163-HI	0.285								87[d]	41[d]	–
SWP 9571-HI[b]	0.220								66[d]	44[d]	–

[a] The listed values are gaussian FWHM after deconvolution of the instrumental broadening of 30 km s^{-1}.
[b] Quiescent spectrum taken at an earlier epoch.
[c] When the Mg II k line profile at flare peak was refit by four gaussians in which the integrated fluxes and widths of three of the gaussians were constrained to the mean quiescent values for the G star, K star, and interstellar medium, the FWHM of the flare component (corrected for instrumental broadening) is 66 km s^{-1}.
[d] C IV 1548 Å line.

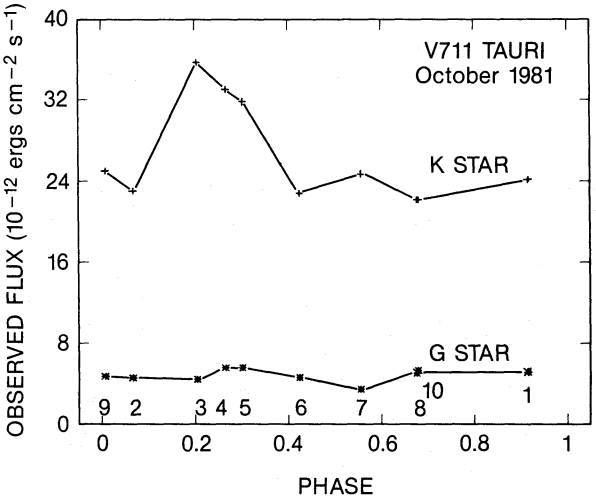

Fig. 2. Integrated Mg II k line fluxes for the K and G stars are presented as a function of orbital phase for V711 Tau during 2–7 October 1981. The Mg k line fluxes for each star were obtained from multi-gaussian fits to the line profiles. The time sequence is indicated by the numerical sequence at the bottom of the figure

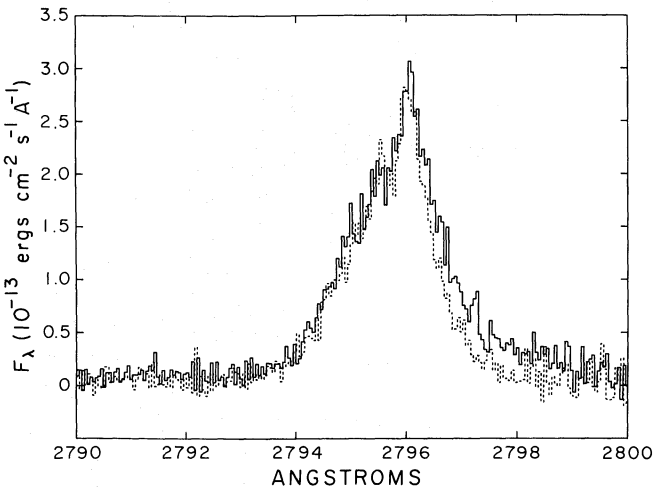

Fig. 3. Observed Mg II k line profiles at flare peak (phase 0.204, solid line) and 7 hours later (phase 0.303, dashed line)

with this data set. To estimate the uncertainty produced by a possible non-gaussian wing (whether intrinsic or plage-induced), we performed a series of fits with an additional line wing component similar to that seen at other phases over the range of possible wavelengths. No position of the additional component affected the centroid or width of the flare component derived above by more than 10 km s^{-1}.

We also analyzed the C IV 1548 Å line in the underexposed high-dispersion spectrum SWP 15163 (phase 0.285) using the same type of multigaussian fit as for the Mg II k line. An unconstrained two-gaussian fit above a quadratic background (Fig. 5) consists of two components separated by 120 ± 10 km s^{-1}, compared to the predicted orbital velocity separation of 108 km s^{-1}. The line flux ratio of about 6 is the same as the ratio of the K and G star Mg II k line fluxes during the flare. While the data are too noisy to separate the K star component into separate quiescent and flare gaussians, the velocity separation between the components for each star is larger than predicted separation by +12 km s^{-1}, a value similar to +15 ± 5 km s^{-1} found for the Mg II k lines during the flare. Unfortunately the data are

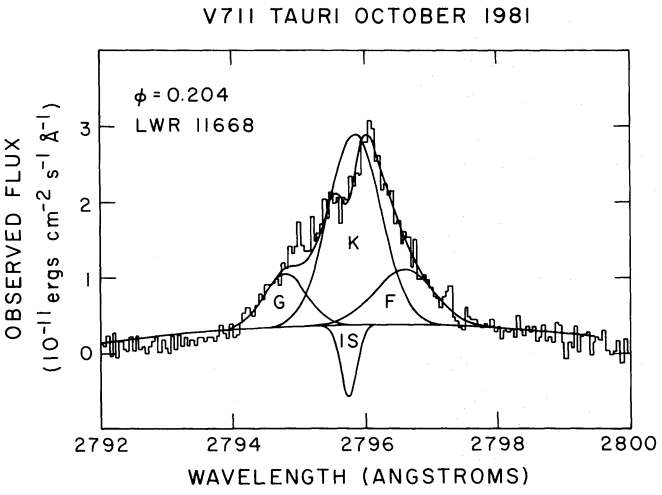

Fig. 4. The observed flare peak Mg II k line profile (phase 0.204) and a four gaussian fit for which the strength and width of three of the gaussians are constrained to be the mean quiescent values for the G star, K star, and interstellar medium, and the radial velocities are those predicted for this phase. The parameters of the fourth gaussian (F) are unconstrained and can be ascribed to the flare. It is centered at $90 \pm 30\,\mathrm{km\,s^{-1}}$ relative to the K star

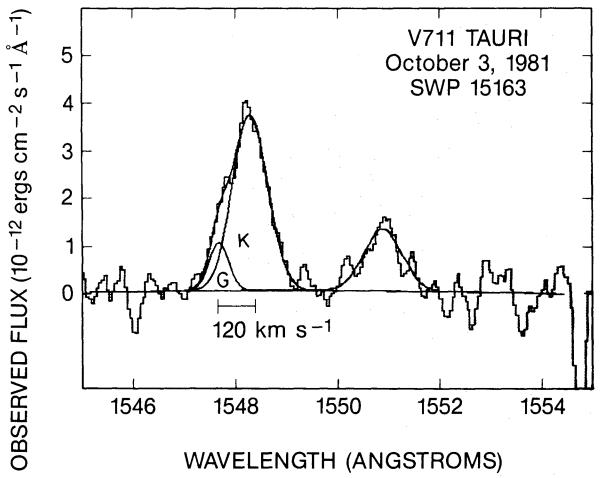

Fig. 5. Observed C IV 1548 Å and 1551 Å line profiles and gaussian fits to these profiles at phase 0.285 during the flare. The taller gaussian component of the 1548 Å line presumably represents the K star emission and the shorter gaussian the G star. The radial velocity separation of the centroids of these gaussians is about $120\,\mathrm{km\,s^{-1}}$, consistent with the $108\,\mathrm{km\,s^{-1}}$ predicted radial velocity separation of the G and K stars. The 1550 Å line is too weak to be fit with more than one gaussian

too noisy to assign much confidence to this result. The C IV doublet flux from both stars in spectrum SWP 15163-HI ($f_{\mathrm{C\,IV}} = 5.6\,10^{-12}\,\mathrm{erg\,cm^{-2}\,s^{-1}}$) is essentially the same as the total C IV flux measured in spectrum SWP 15164-LO ($f_{\mathrm{C\,IV}} = 5.25\,10^{-12}\,\mathrm{erg\,cm^{-2}\,s^{-1}}$) that was obtained afterwards.

The H I Lα profile in SWP 15163 includes emission from both stars and absorption due to neutral hydrogen and deuterium by the intervening interstellar medium. The interstellar hydrogen column density in this line of sight is low ($\log N_{\mathrm{H}} = 18.0 - 18.2$ according to Murthy et al., 1987), and the intrinsic stellar profile is broad; thus most of the stellar profile is unaffected by the interstellar absorption. The intrinsic shapes of the combined Lα profiles of both stars are unknown, but we expect them to be roughly gaussian (Anderson and Weiler, 1978). We therefore fit a gaussian emission component to the Lα wings, excluding from the fit the line core. For comparison, we applied the same procedure to a non-flare spectrum (SWP 9571) that was obtained at a different epoch but a similar phase. The observed shapes of the line cores in Fig. 6 were matched by subtracting from the emission gaussian fit to the line wings two gaussians centered at the expected wavelengths of the hydrogen and deuterium Lα absorption along the line of sight. This procedure is purely illustrative and does not change our estimate of the stellar Lα flux. Clearly there is an enhancement in the Lα flux between the flare and the non-flare spectrum, but the width and wavelength of the flare emission are not significantly different from the non-flare emission. The estimated intrinsic stellar Lα flux during the flare is given in Table 3, together with the corresponding preflare flux estimated from the nonflare spectrum.

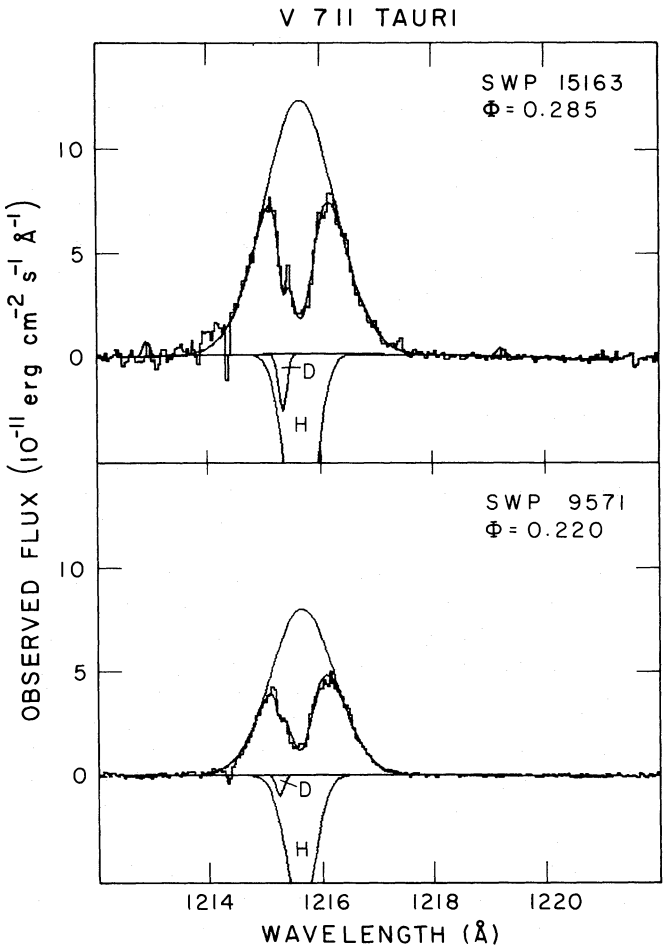

Fig. 6. Observed Lyα line profiles during the flare (phase 0.285) and at a quiescent time (phase 0.220). The observed profiles are fitted with an emission gaussian (the assumed intrinsic combined stellar emission line), which is determined by fitting only the line wings. We subsequently estimated the degree of interstellar hydrogen (H) and deuterium (D) absorption with gaussian components, holding the stellar emission fixed. The flux at line center does not go to zero because of weak geocoronal emission

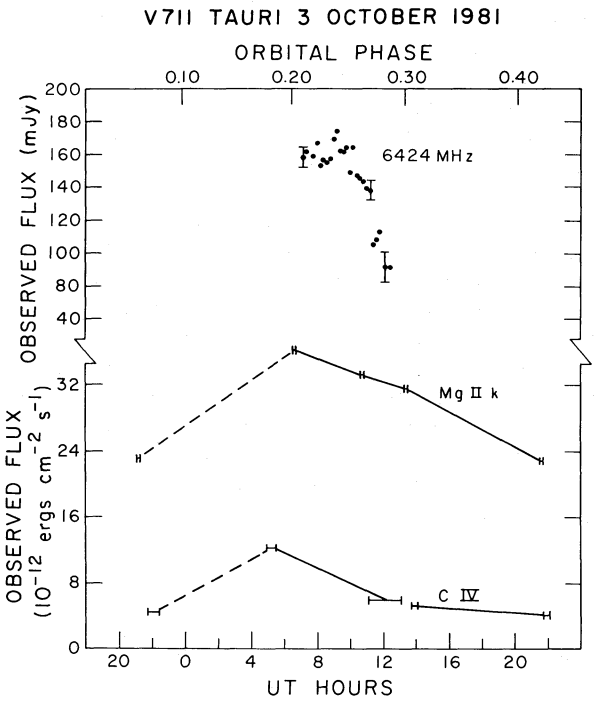

Fig. 7. Comparison of radio and integrated ultraviolet emission line fluxes during the 3 October 1981 flare on V711 Tau. The top panel contains 6424 MHz radio flux measurements from Algonquin Radio Observatory with typical $\pm 1\sigma$ error bars included. The lower panel shows integrated Mg II k line fluxes for the K star and integrated C IV fluxes for both stars together. The horizontal error bars show the duration of the IUE exposures. The dashed lines connecting the first two data points indicate that the time variation of the Mg II and C IV fluxes between the two data points is unlikely to be linear

2.4. Radio emission

V711 Tauri was monitored on 2–5 October 1981 by the Algonquin Radio Observatory with a bandwidth of 200 MHz centered at 6424 MHz. A portion of these data is plotted as in Fig. 7. The observed fluxes are large, symptomatic of flare activity, although less than those of several major radio flares (Feldman, 1983). A general correlation of high radio with Mg II and Lα flux was seen previously in the 24 September 1976 flare on V711 Tauri (Weiler et al., 1978), and the close correlation of strong radio flux with enhanced emission in Hα and Ca II is well known (e.g. Bopp, 1983). There were no radio observations at the time of the flare peak spectra (0455–0642 UT), but the radio fluxes at 0700–1030 UT lie in the range 145–175 mJy followed by a rapid decrease to 90 mJy by 1200 UT. The rapid decline can be contrasted with the gradual decline in the Mg II k line flux at the same time. The Algonquin data exhibit high flux levels on 2, 4, and 5 October, suggesting a prolonged radio flaring episode extending over at least 4 days.

2.5. Optical photometry

The optical light curve of V711 Tau was monitored at several observatories before, during, and after the IUE observations. The data available for the 1981–2 season are summarized in Paper I and in Sarma et al. (1985). In the latter paper evidence is presented for a double minimum in the light curve beginning in 1980.7, indicating the emergence of a new spot group at low latitude. Modelling in Paper I of the visual light curve at epoch 1981.8 indicates a high latitude spot crossing at phase 0.17 and a low latitude spot crossing at phase 0.54. Applying a Doppler imaging technique to optical spectra taken at this epoch, Vogt and Penrod (1983) concluded that large spots (or spot groups) crossed the central meridian at phases 0.23 (high latitude) and 0.53 (low latitude), in agreement with Paper I.

During October 1981, the data summarized in Paper I show that mean visual magnitude of V711 Tau (correcting for the optical companion 6.″5 away) at phase 0.2 (the phase of the flare peak) was 5.87 $\pm$ 0.015. Independent data presented by Sarma et al. for epoch 1981.87 place the visual magnitude at 5.855 $\pm$ 0.015 for phase 0.2 (assuming that the visual magnitude of the comparison star 10 Tau is 4.29). These two independent data sets are thus in good agreement. The visual magnitudes obtained within one day of the flare by the IUE fine error sensor (FES) and at Hopkins and Catania Observatories both agree with the mean visual magnitudes for phase 0.2 previously cited, except for two FES magnitudes at phases 0.183 and 0.204 (see Table 1). These measurements at flare peak lie 0.06 and 0.10 magnitudes, respectively, above the mean magnitude of 5.87 for this phase (see Fig. 8 of Paper I). While the FES magnitudes are much less accurate than ground-based photometry, the enhancement of $\sim$0.08 magnitudes at flare peak might be real. If so, the increase in the visual luminosity is $1.4\,10^{32}$ erg s^{-1}, which is 10 times larger than the enhancements in the luminosity of the chromospheric and transition region lines. Thus accurate, simultaneous visual photometry is essential in future studies of the energy budget of RS CVn flares.

3. Physical properties of the flaring plasma

3.1. Estimates of electron densities

The only detected density-sensitive intersystem lines (see Table 3) are C III] 1909 Å, O III] 1666 Å and Si III] 1892 Å. Unfortunately the O III] lines are severely blended with Al II and Fe II lines and are not usable. The flux in the C III] 1909 Å line barely increased during the flare (see Fig. 8). Details concerning the behavior of the Si III] 1892 Å line were discussed by Byrne et al. (1987, Paper VI). As shown in Fig. 8, the C III 1175 Å multiplet is enhanced during the flare, but there is concern about opacity effects in this line (cf. Paper VI) and the poorly determined IUE flux calibration at this wavelength. Thus this line should not be used as the primary density diagnostic.

The electron density in the flaring plasma was estimated from the observed Si III] 1892 Å/C III] 1909 Å and Si IV (1396 + 1403 Å)/C III] 1909 Å flux ratios. These lines form where the electron temperature is about $6\,10^4$ K. We list in Table 6 these flux ratios for the preflare spectrum (SWP 15158-LO) and for the flare enhancement spectrum (the flare peak spectrum [SWP 15161-LO] minus the preflare spectrum). This table also lists the electron densities determined from these ratios using the Si IV/C III] calibrated ratios given in Paper VI (the solid line in Fig. 7 of Paper VI), and the Si III/C III] ratios normalized to the observed quiet Sun (Table 1 in Keenan et al., 1987). The derived flare electron density, $N_e = 1\,10^{11}$ cm^{-3}, is an order of magnitude larger than the preflare value. The electron densities derived from the C III] 1909 Å/C III 1175 Å line flux ratios (see Table 6) are

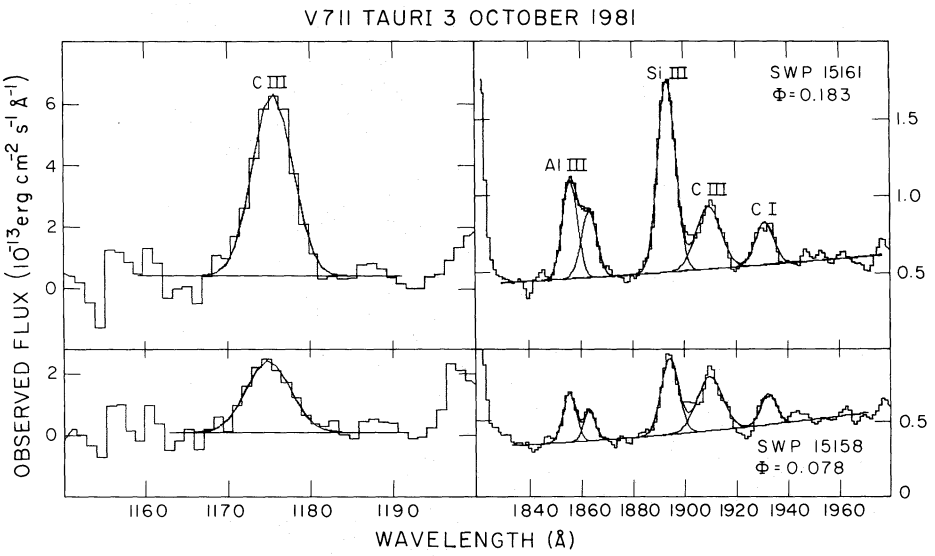

Fig. 8. Portions of the IUE short wavelength spectra obtained near the flare peak (top) and prior to the flare (bottom) are shown on the same scale. Gaussian fits for important spectral features are illustrated

consistent with those derived using the order diagnostics. We therefore adopt $N_e = 1\,10^{11}\,\mathrm{cm}^{-3}$ for the electron density of the flaring plasma.

The flare emission measure distribution, $EM = \int_{\Delta h} N_e^2\,dh$, is shown in Fig. 9, and the emission measures of individual lines are given in Table 7. The definition of EM is that discussed by Brown et al. (1984) and relates to a temperature range of $\Delta \log T = \pm 0.15$. This conventional emission measure is a factor of 3 larger than the formulation used in Paper VI. The emission line integrated surface flux, F_*, and EM are related by

$$F_* = \frac{6.8\,10^{-22}}{\lambda(\mathrm{cm})}\frac{\Omega_{12}}{\omega_1}\alpha\frac{N_1}{N_{\mathrm{ion}}}\frac{N_E}{N_H}\int_{\Delta h} N_e^2 g(T)\,dh. \quad (1)$$

When metastable levels are involved, the full population solution was used. Here Ω_{12} is the collision strength (Seaton, 1962), ω_1 is the statistical weight of the lower level, N_E/N_H is the elemental abundance, N_1/N_{ion} is the fractional population in the ground state, and $\alpha = A_{21}/(A_{21} + C_{21})$ is the probability of radiative decay. These quantities are given in Table 7. The function $g(T)$ is

$$g(T) = T_e^{-1/2}\exp\left(-\frac{W_{12}}{kT_e}\right)\frac{N_{\mathrm{ion}}}{N_E}, \quad (2)$$

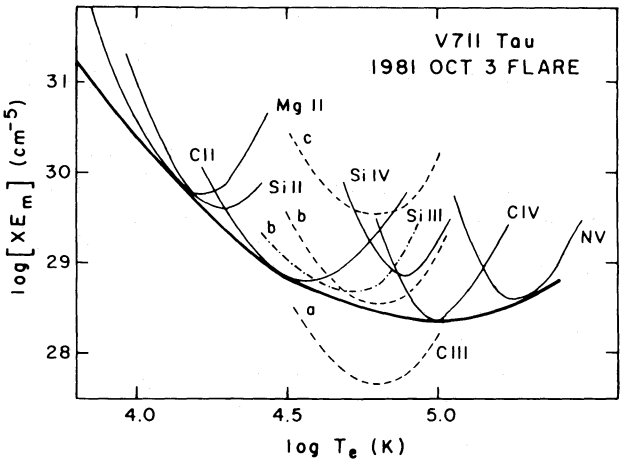

Fig. 9. The emission measure distribution of the V711 Tau flare. The quantity XEM, where X is the fractional surface area coverage of the emitting plasma and EM is the emission measure, is plotted versus log T_e. The thick solid curve is the adopted mean emission measure distribution. The thin curves represent the contribution functions of particular emission lines. Three dashed curves for C III] 1909 Å correspond to different electron densities, a: $10^{10}\,\mathrm{cm}^{-3}$, b: $10^{11}\,\mathrm{cm}^{-3}$, and c: $10^{12}\,\mathrm{cm}^{-3}$. For Si III] 1892 Å a dot-dash curve is calculated for an electron density of $10^{11}\,\mathrm{cm}^{-3}$

Table 6. Estimates of electron densities at $T = 6\,10^4$ K

Diagnostic used	Line flux ratios		Log N_e		Reference
	Preflare	Flare enhancement	Preflare	Flare enhancement	
Si IV (1396 + 1403 Å) / C III] 1909 Å	3.3	40	10.0	11.0	Paper VI
Si III] 1892 Å / C III] 1909 Å	1.0	13	9.5	11.0	Keenan et al. (1987)
C III] 1909 Å / C III 1175 Å	0.33	0.024	9.6	10.8	Doyle et al. (1980)

Table 7. Atomic data and derived emission measures

Ion	λ (Å)	F_* (10^5 erg cm^{-2} s^{-1})	α	Ω	ω_1	$g(T_m)$	N_1/N_{ion}	N_E/N_H	EM (cm^{-5})	log T_m (K)
N V	1240	1.8	1.0	7.2	2	3.1(−4)	1.0	8.0(−5)	3.8(28)	5.2
C IV	1549	6.9	1.0	11.2	2	6.4(−4)	1.0	2.5(−4)	1.8(28)	5.0
Si IV	1400	1.8	1.0	16.4	2	2.2(−4)	1.0	4.0(−5)	5.2(28)	4.9
C III	1909	0.046	0.30[a]	0.95	1	9.8(−4)	0.544[a]	2.5(−4)	3.5(27)[a]	4.75
			0.043[b]				0.466[b]		2.8(28)[b]	
			0.0045[c]				0.457[c]		2.8(29)[c]	
Si III	1892	0.61	0.76[a]	3.2	1	8.5(−4)	0.83[a]	4.0(−5)	2.5(28)[a]	4.7
			0.54[b]				0.81[b]		3.6(28)[b]	
C II	1335	3.3	1.0[b]	6.5	2	1.6(−4)	0.84[b]	2.5(−4)	6.1(28)[b]	4.5
Si II	1814	1.0	1.0	23	6	6.6(−5)	1.0	4.0(−5)	2.7(29)	4.3
Mg II	2800	19.1	1.0	35.4	2	2.6(−4)	1.0	4.0(−5)	>4.4(29)	4.2

[a] $N_e = 10^{10}$ cm^{-3}.
[b] $N_e = 10^{11}$ cm^{-3}.
[c] $N_e = 10^{12}$ cm^{-3}.
Note: $g(T_m)$ is the value of $g(T)$ at the peak of this function, where $T_e = T_m$ (see Brown et al., 1984, Sect. 4.1). F_* is the emission line surface flux computed from the observed flux enhancements in Table 3 and the conversion factor $F_*/f = 0.91\,10^{17}$ for the K 1 IV star given in Table 8 of Paper III

where W_{12} is the excitation energy. The emission measure loci for the C III] and Si III] intersystem lines are calculated for a range of electron densities and show best agreement with the mean emission measure distribution indicated by the resonance lines for $N_e \sim 10^{11}$ cm^{-3}.

3.2. *Flaring volume*

For a collisionally-excited emission line the power radiated, P, is related to the emitting volume, dV, by

$$P = h\nu_{ij} N_i N_e C_{ij}\, dV, \tag{3}$$

where $h\nu_{ij}$ is the energy of the transition, C_{ij} is the collisional excitation rate coefficient, N_e is the electron number density, and N_i is the ion number density in the lower level.

The volume of the flare emitting region can be estimated using the atomic data given in Paper VI, the flare emission line luminosities in Table 7 (P and ΔL_{flare} are equivalent), and $N_e \approx 1\,10^{11}$ cm^{-3}. Based on the C IV or Si IV emission lines, the emitting volume is found to be $8\,10^{29}$ or $36\,10^{29}$ cm^3, respectively. The transition-region emitting volume of the flare was roughly 200 times smaller than that of the quiescent atmosphere, due to the N_e^{-2} dependence of dV.

In Paper VI, we considered a large loop model for active region emission in which the loop volume, V_{loop}, and footpoint separation, D, were related by

$$V_{loop} \sim 0.01\pi^2 (D/2)^3. \tag{4}$$

When this model is applied to the V711 Tau flare, the footpoint separations for single loops are $4.1\,10^{10}$ and $6.5\,10^{10}$ cm based on the C IV and S IV lines, respectively. These separations correspond to 15–24% of the K star radius, analogous to the largest solar active region loops, given the lower surface gravity of the K star. Nothing in our data suggests that only one loop is flaring, while the radio variability suggests the presence of several flaring loops. Such loops would still be large under the above assumptions, with footpoint separations of $1\,10^{10}$ cm for 10 identical loops and $6\,10^9$ cm for 100 loops.

3.3. *Radiative luminosity*

The mean emission measure distribution shown in Fig. 9 can be used to calculate the upper chromospheric and transition region radiative luminosity. The radiative loss per unit area of the stellar surface ΔF_R over a temperature range $\Delta \log T = \pm 0.15$ is given by

$$\Delta F_R = 1.14 EM(T) P_{rad}(T). \tag{5}$$

Using the power loss function $P_{rad}(T)$ of McWhirter et al. (1975), we estimate the total luminosity from plasma in the temperature range $4.0 < \log T_e < 5.3$ to be $1.2\,10^{32}$ erg s^{-1}. If the Raymond et al. (1976) cooling curve is used instead, this becomes $1.7\,10^{32}$ erg s^{-1}. Since the emission measure is per unit surface area, this result is independent of the fractional surface area coverage, X, of the flare. The duration of the flare is not well defined. The Mg II emission flux (see Fig. 7) still shows a substantial enhancement six hours after the "flare peak", but it returned to a normal level after 15 hours. The SWP spectra show that quiescent levels in C IV and C II emission are reached after seven hours. These data suggest 1/e decay time scales of roughly 5 hours for the transition region lines and perhaps 12 hours for the chromospheric lines, implying a total flare radiative energy in the above temperature range of at least $2.4\,10^{36}$ erg. These time scales are much longer than the 10–20 minute time scales typical of solar compact flares (Canfield et al., 1980), but are comparable to solar two-ribbon flares. Bruner and McWhirter (1988) show that the total flare radiative energy (excluding hydrogen) for $4.0 < \log T_e < 8.0$ can be estimated from the C IV flux to be roughly $5\,10^{36}$ erg.

The flare peak luminosities of individual emission lines in Table 8 indicate that the V711 Tau flare is intermediate in strength between the λ And and UX Ari flares, but all three stellar

Table 8. Comparison of flare peak enhancement luminosities ΔL_{flare}

Spectral feature	V711 Tau[a] 1981 Oct. 3 (10^{30} erg s^{-1})	UX Ari[b] 1979 Jan. 1 (10^{30} erg s^{-1})	λ And[c] 1982 Nov. 6 (10^{30} erg s^{-1})	AY Cet 1983 Dec. 6 (10^{30} erg s^{-1})	Sun[d] 1973 Sept. 5 (10^{24} erg s^{-1})
N V 1240 Å	0.23	0.66	0.041	0.10	0.49
C IV 1550 Å	0.87	1.9[e]	0.31	0.80	6.6
Si IV 1400 Å	0.23	0.74	0.10	0.29	3.8
Al III 1860 Å	0.05	0.15[e]	0.021	–	0.12
C III 1175 Å	0.24	0.65	0.14	–	1.2
Si III 1892 Å	0.08	0.23	0.028	–	–
O III 1666 Å	0.04	–	0.021	–	–
C II 1335 Å	0.41	1.3[e]	0.010	0.19	4.7
Si II 1812 Å	0.13	0.61[e]	0.062	0.12	0.12
O I 1304Å	0.23	0.60	0.12	0.15	0.57
C I 1657 Å	0.01	–	0.021	0.03	0.60
Mg II h and k	2.41	13	1.34	3.0	(2.3)[f]
He I 1640 Å	0.12	1.0[e]	0.062	0.14	0.19
H I 1216 Å	8.1	(43.3)[f,g]	2.13	3.0	7.5[g]
Sum	13.2	(64.1)	4.5	7.82	(28.2)

[a] Assuming a distance of 31 pc and no correction for interstellar absorption.
[b] Assuming a distance of 50 pc and no correction for interstellar absorption.
[c] Assuming a distance of 24 pc and no correction for interstellar absorption.
[d] From Canfield et al. (1980).
[e] Assuming a flare enhancement factor of 5.5 for transition region lines and 2.5 for chromospheric lines.
[f] Assuming a flare flux enhancement ratio Lα/Mg II = 3.33.
[g] Corrected for interstellar Lα absorption

flares are orders of magnitude larger than the large solar flare of 5 September 1973.

The flare peak luminosity in the ultraviolet emission lines may also be compared with the luminosity in other bands. For example, the enhanced flux in the ultraviolet continuum (1580–1630 and 1750–1780 Å) bands is about 1% the sum of the ultraviolet emission lines. However the FES visual magnitude near the flare peak was $V = 5.79$ compared with $V = 5.87 \pm 0.015$, the mean visual magnitude at phase 0.2. The reality of this enhancement is in doubt because of the uncertainty whether the visual companion of V711 Tau was included. If the visual flux of V711 Tau itself brightened, then the luminosity in the visual band increased by about $1.4\,10^{32}$ erg s^{-1}, 10 times larger than in the ultraviolet emission lines but a value similar to the luminosity from plasma in the temperature range $4.0 < \log T_e < 5.3$.

3.4. Systematic and turbulent motions during the flare

As described in Sect. 2.3, we first modelled the Mg II k lines profiles during the flare with four unconstrained gaussians: three to represent emission from the K star, the G star, and an additional component that we call P, and the fourth to represent absorption by the interstellar k line. The observed profiles (before modelling) showed no significant asymmetries as were observed during the 1 January 1979 flare on UX Ari (Simon et al., 1980). In Table 5 the fitted line widths (FWHM) using the first modelling procedure are given for both the K and G stars, after deconvolving the instrumental broadening. These data show the systematic narrowing of the K star profile with time, whereas the width of the G star profile was constant. The C IV 1548 Å profile component ascribed to the K star was also broader during the flare compared to a quiescent profile obtained at a similar phase but different epoch (see Table 5). These data indicate that the flare occurred on or near the K star. The additional broadening beyond the quiescent values corresponds to ~ 60 km s^{-1} in Mg II at flare maximum and C IV during the decay phase.

The Mg II data are consistent with the flare occurring over a large portion of the K star with the substantial broadening as evidence for large-scale line of sight motions associated with the plasma heating. We believe, however, that this explanation is unlikely since: the density-sensitive diagnostics (see Sect. 3.2) indicate that the flaring volume was very small, roughly 200 times smaller than the quiescent atmosphere; the gaussian component identified with the K star was shifted 15 ± 5 km s^{-1} relative to the expected radial velocity of the K star, suggesting systematic motions; and solar flares seen in the ultraviolet and X-rays typically occur in small loop structures. We therefore refitted the flare peak k line profile with four gaussians in which three were constrained to be centered at the predicted radial velocities of the K star, G star, and interstellar medium, and the integrated fluxes of the K and G stars were constrained to be their mean quiescent values. The unconstrained fourth gaussian represents the flare alone (see Fig. 4).

As described in Sect. 2.3, the flare gaussian is shifted 90 ± 30 km s^{-1} relative to the center of mass of the K star, and the FWHM of the flare component, corrected for instrumental broadening, is 66 km s^{-1}, which corresponds to a most probable rms speed of 49 km s^{-1} if the turbulent motions are presumed isotropic. Since the flare presumably covered only a small portion of the star, the broadening of the flare component cannot be due

to rotational smearing, but instead must be due to line-of-sight motions. There is a net downflow of $\approx 90\,\mathrm{km\,s^{-1}}$ if the flare occurred on the central meridian of the K star, $\approx 50\,\mathrm{km\,s^{-1}}$ if it occurred on the equator at the receding limb (the projected rotational velocity at the equator, $v \sin i = 38\,\mathrm{km\,s^{-1}}$ (see Paper III), or zero velocity if the flare occurred in a corotating structure lying 1.4 R_* above the equator at the receding limb. Any combination of downflow and rotation with large line-of-sight motions can also explain the flare Mg II emission, however, the flare was still observable $8\frac{1}{2}$ hours (0.13 in phase) after its first detection so that it could not have been located initially at or above the receding limb. Redshifts in chromospheric lines associated with material downflows and turbulent motions with energy content comparable to the radiative losses are often detected during solar flares. Indeed, such motions could be an intermediate energy storage mechanism (Bornmann, 1987).

In Paper IV we called attention to a flare on AR Lac that was also indicated by a 50% flux enhancement in the Mg II k line. There are some interesting similarities between the AR Lac flare and the V711 Tau flare. Unfortunately only one flare spectrum is available for AR Lac, so its identification as a short-lived flare rather than a long-lived plage is uncertain. The AR Lac flare component is comparable in width to that we have found for V711 Tau but is shifted to shorter wavelengths relative to the K star. In Paper IV this shift is interpreted as due to the flare occurring near the approaching limb of the K star, but any combination of rotational Doppler shift and flows could explain the observed Doppler shift.

Without additional information we cannot say where on the K star of V711 Tau the flare occurred. At this epoch the light curve of V711 Tau was rapidly changing (Paper I, Sarma et al.), implying rapid rearrangement of spots and magnetic flux, which might be conducive to flaring. Large solar flares generally occur above sunspots where the magnetic fields and field gradients are large. If this solar analogy is a useful guide, then we expect that the flare occurred above a spot (or spot group). A likely candidate is spot 1 (see Fig. 10 of Paper I), which was located near disk center at phase 0.2, rather than spot 2, which was then located at the advancing limb and would have produced a rotational blue shift. Smaller spots elsewhere on the disk cannot be ruled out, nor can the possibility that the flare disappeared behind the limb between phases 0.310 and 0.424. If the flare occurred above spot 1 near disk center, then the observed $90 \pm 30\,\mathrm{km\,s^{-1}}$ redshift is due entirely to downflow and not rotation. Since the flare detected in the ultraviolet covered only 0.5% of the observable stellar surface, as indicated by the density-sensitive line ratios, then the flare is much smaller than spot 1, which covered 18% of the stellar surface at that time.

The flux of kinetic energy into the chromosphere due to the downflow and turbulence observed in the Mg II k line near the flare peak can be computed assuming a downflow velocity $v \leq 90\,\mathrm{km\,s^{-1}}$, an rms speed $\xi_t = 49\,\mathrm{km\,s^{-1}}$, a flare surface area $A = 1.2\,10^{21}\,\mathrm{cm^2}$ (corresponding to 0.5% of the surface area of the K star), and a neutral gas. The kinetic energy flux is

$$f_{\mathrm{KE}} = \tfrac{1}{2}P(v^2 + \xi_t^2)vA \leq 1.5\,10^{30}\,P\,\mathrm{erg\,s^{-1}}. \quad (6)$$

Here P is the gas pressure where the Mg II lines are formed. The density-sensitive line ratios previously discussed provide an estimate of $N_e = 1\,10^{11}\,\mathrm{cm^{-3}}$ at $T = 6\,10^4\,\mathrm{K}$. Thus at $T = 6\,10^4\,\mathrm{K}$ in the flare, $P = 1.6\,\mathrm{dyne\,cm^{-2}}$. Models of solar flares (e.g. Machado et al., 1980) typically show pressures increasing inwards by a factor of ~ 30 between the layers where the transition region lines are formed and where the Mg II lines are formed. Thus we estimate that $f_{\mathrm{KE}} \leq 1.5\,10^{30}\ (1.6)(30) \leq 1\,10^{32}\,\mathrm{erg\,s^{-1}}$, within a factor of 2 of the estimated flare radiative luminosity (ΔL_{rad}) for the limited temperature range $4.0 \leq \log T_e \leq 5.3$. We have thus found three energy fluxes near flare peak with essentially the same value: the kinetic energy flux (f_{KE}), the radiative luminosity (ΔL_{rad}), and the luminosity (ΔL_v) corresponding to the possible V-band brightening. This coincidence suggests that the flare process naturally produces equipartition among these various energy modes, for example, if the kinetic energy flux were responsible for most of the nonradiative heating in the photosphere or in the temperature range $4.0 < \log T_e < 5.3$. Future observing campaigns therefore should look for systematic flows at all levels in the atmosphere.

3.5. *Analysis of the radio emission*

Radio emission from RS CVn systems has been observed at many wavelengths and recently with VLBI techniques (e.g. Feldman, 1983; Lestrade et al., 1984; Mutel et al., 1985). What makes the present radio observations important and perhaps unique is that they are concurrent with the ultraviolet spectra that provide information on the size of the flaring loop(s) and their location on the K 1 IV star in the V711 Tau system.

Prior to VLBI measurements, many authors analyzed the 1–15 GHz flare radiation as gyrosynchrotron radiation from mildly relativistic electrons (e.g. Owen et al., 1976). Occasional observations of short duration, highly circular polarized events have been interpreted as coherent emission (e.g. Brown and Crane, 1978), which today would be ascribed to an electron cyclotron maser. The power of the VLBI technique is that it allows submilliarcsecond resolution or imaging and thus realistic estimates of the source brightness temperature. Mutel et al. (1985) proposed an "expanding coronal loop" model. At the onset of a flare (Phase I in their model) optically thick gyrosynchrotron emission with source brightness temperature $T_B = T_{\mathrm{eff}} = 1 - 6\,10^{10}\,\mathrm{K}$ is produced by mildly relativistic electrons ($\gamma = 2 - 10$, corresponding to energies $E = 1 - 5\,\mathrm{MeV}$) trapped in compact loops ($B \sim 100\,\mathrm{Gauss}$) located close to the surface of the active star in the RS CVn system. The authors speculated that these compact loops would be associated with a starspot or spot group on the active star.

Is the 3 October 1981 flare on V711 Tau consistent with Phase I of the expanding coronal loop model? We do not have multifrequency, polarization, or VLBI measurements, but the 6.4 GHz fluxes ($S_\nu = 90 - 170\,\mathrm{mJy}$) during the flare are typical of those analyzed by Mutel et al. (1985), the radio flare was coincident in time with the ultraviolet flare, and both decayed together although with different time scales. Thus both structures could have been produced in the same (or adjacent) compact loop. In addition to the October 3 microwave flare, which exhibited a 2-hour decay time scale (see Fig. 7), another well-observed flare exhibited a steady decay from 110 to 50 mJy between 0830 and 1100 UT on October 4. Finally, the ultraviolet flare was likely associated with the large starspot near disk center so that the microwave emission was likely also associated with this spot.

We have shown (Sect. 3.2) that the emission measures and electron densities are consistent with emission from a semicircular loop with footpoint separation of $5\,10^{10}\,\mathrm{cm}$ ($=0.18\,R_* = 0.10\,\mathrm{milliarcsec}$) and volume $\sim 2\,10^{30}\,\mathrm{cm^3}$. The projected area of

this loop is $\approx 0.135\, D^2 = 3.4\, 10^{20}\,\mathrm{cm}^2$, nearly independent of its orientation. If we assume that all of the microwave emission ($S_\nu = 160\,\mathrm{mJy}$) originated in the loop, then

$$T_B = \frac{c^2 d^2 S_\nu}{2k\nu^2 A} \approx 3.5\, 10^{12}\,\mathrm{K}. \quad (7)$$

If instead, we assume that the microwave emission was from loops that cover the entire disk of the K 1 IV star, then $A = \pi R_*^2 = 2.3\, 10^{23}\,\mathrm{cm}^2$ and $T_B = 5\, 10^9\,\mathrm{K}$. The corresponding typical electron energies are $E_0 = kT_B = 300\,\mathrm{MeV}$ or 0.43 MeV, respectively. The first value of T_B is much larger than inferred from the VLBI data and is uncomfortably large for incoherent gyrosynchrotron emission and above the inverse Compton limit. It would imply maser emission or plasma emission for which we have no other evidence. The second estimate of T_B is somewhat low compared to typical values from VLBI observations of flares.

Let us reverse the argument and ask what area on the K 1 IV star is consistent with the largest value of T_B measured by Mutel et al. (1985) for a *resolved* flare, $T_B = 2\, 10^{10}\,\mathrm{K}$ derived for the July 1983 flare on HR 5110. The corresponding surface area is $A = 6\, 10^{22}\,\mathrm{cm}^2 \approx 1.4\, A_{\mathrm{spot}}$, where A_{spot} is the surface area of the spot near disk center (see Paper I and Vogt and Penrod, 1983) at the time of the flare. These arguments lead us to conclude that the microwave emission was from a set of loops originating in the spot, but the uncertainty in the estimated value of T_B would suggest that the surface area of the loops is the same as the spot to within a factor of 2 or perhaps 3. A rough estimate of the magnetic field strength near the $\tau_{6.46\,\mathrm{Hz}} = 1$ level is 5 – 10 Gauss for an electron energy index $\delta = 2 - 3$ and angle between the electron velocity and magnetic field $\theta = 60°$ (Dulk, 1985, Eq. (42)).

Until this point we have assumed that the 10^5 K plasma responsible for the ultraviolet emission lines uniformly filled a semicircular loop of volume $\sim 2\, 10^{30}\,\mathrm{cm}^3$. During solar flares plasma of this temperature generally exists near the footpoints of the loops and consists of matter evaporated from the underlying dense chromosphere by some rapid heating process. The rest of the loop is filled with hot or nonthermal plasma. If this scenario is applicable to RS CVn flares, then the same volume of 10^5 K plasma should lie near the footpoints of flux tubes. If we require that the 10^5 K plasma partially fill the same flux tubes from which the microwave emission arises, then the 10^5 K plasma occupies about 0.01% by volume of these flux tubes.

This model is not unique, but it is consistent with *all* of the data and solar analogy. It also involves the minimum of geometrical assumptions as now all of the presumably interconnected phenomena (starspots, ultraviolet emission, radio emission, downflows and turbulence) occur at the same place on the surface of the active star in V711 Tau.

4. Conclusions

Our simultaneous observations of a large flare from the V711 Tau system at optical, ultraviolet, and radio wavelengths lead to several important conclusions and a working model for flares on RS CVn systems:

1. The observed chromospheric and transition region emission line profiles indicate that the flare occurred on the K subgiant star. The lack of significant line asymmetries suggests that the flare emission component was broad, and multigaussian fits to the Mg II k line profile indicate that the FWHM of the flare profile corrected for instrumental broadening was $66\,\mathrm{km\,s^{-1}}$. The combined rotational and systematic flow velocity of the flaring plasma was $90 \pm 30\,\mathrm{km\,s^{-1}}$. This redshift could be due entirely to a corotating structure lying 1.4 stellar radii above the receding limb at the equator, or to a $90\,\mathrm{km\,s^{-1}}$ downflow near disk center, or to a combination of the two motions. Since a large starspot was located at the center of the visible hemisphere of the K star at the time of the flare, analogy with solar flares suggests that the flare most likely occurred above this starspot. We estimate that the flux of kinetic energy due to the downflow and turbulence was $\leq 1\, 10^{32}\,\mathrm{erg\,s^{-1}}$ near the flare peak.

2. The electron density in the flaring plasma is found to be about $1\, 10^{11}\,\mathrm{cm}^{-3}$ at electron temperatures of $\sim 6\, 10^4$ K. This electron density is a factor of 15 larger than the global average density preceding the flare.

3. The volume of the flaring plasma at $\sim 10^5$ K was roughly $2\, 10^{30}\,\mathrm{cm}^3$, a factor of 200 times smaller than the quiescent atmosphere. A simple magnetic loop geometry suggests footpoint separations of about $5\, 10^{10}$ cm, about a factor of 5 times smaller than the spot diameter.

4. The measured luminosity of the flare in the ultraviolet emission lines (including Mg II and Lα) was larger than the 6 November 1982 λ And flare and the 6 December 1983 AY Cet flare but a factor of 5 smaller than the powerful 1 January 1979 UX Ari flare. All of these flares are some 10^6 times more luminous than typical large solar flares. The radiative luminosity was 1.2–$1.7\, 10^{32}\,\mathrm{erg\,s^{-1}}$ in the temperature range $4.0 < \log T_e < 5.3$ at the peak of the flare, and the radiative energy integrated over the duration of the flare in this temperature range was at least 2.4–$3.4\, 10^{36}$ erg. The flux of kinetic energy at the flare peak was $\leq 1\, 10^{32}\,\mathrm{erg\,s^{-1}}$, essentially equal to the radiative luminosity in this temperature range.

5. The 6.4 GHz microwave emission had a flux density and temporal variability consistent with other flares on RS CVn systems that are interpreted as gyrosynchrotron emission from mildly relativistic electrons on the basis of VLBI observations and spectral data. The temporal coincidence with the flare seen in the ultraviolet and the common decrease in flux at radio and ultraviolet wavelengths implies that they are both produced in the same or adjacent magnetic field loops above the starspot. We assume that $T_B = 2\, 10^{10}$ K, and deduce an emitting area 1.4 times the surface area of the spot near disk center, which is plausible if the relativistic electrons are confined by flux tubes emerging from the whole spot area. However, the uncertainty in the assumed value for T_B indicates that the deduced area for the radio emission is uncertain by a factor of 2 and perhaps 3. Solar analogy suggests that the 10^5 K flare plasma is evaporated chromospheric gas near the flaring tube footpoints.

A self-consistent picture of the flare is therefore one in which the flare occurs in magnetic flux tubes that fill the whole starspot, with 0.01% of the flux tubes by volume filled with 10^5 K plasma (presumably near the footpoints) and the rest of the tube volume filled with relativistic electrons with a typical energy of 1.7 MeV. Since this picture is consistent with all of the presumably interconnected phenomena (starspots, ultraviolet emission, radio emission, and downflows) occurring in the same location, we adopt this scenario as our working model for flares on RS CVn systems.

Acknowledgements. We thank the staffs of the NASA (GSFC) and ESA (VILSPA) IUE ground stations for their assistance in obtaining these observations and the staff of the IUE Regional Data Analysis Facility in Boulder (supported by grant NASA5-26409) for their assistance with data reduction. We acknowledge financial support from NASA grant NAG5-82 to the University of Colorado, from the Italian Ministero della Pubblica Istruzione and from the C.N.R. (Gruppo Nazionale di Astronomia) to the Osservatorio Astrofisico di Catania, and from NATO Scientific Affairs Division for a travel grant (No. 386/84) to maintain the collaboration between the three institutions: Armagh Observatory, the Joint Institute for Laboratory Astrophysics, Boulder, Colorado, and the University of Catania. We also thank NASA, ESA and SERC for the allocation of time on IUE, Dr. G. Dulk for discussions concerning analysis of the radio observations, and Dr. T. Ayres and the referee for a careful reading of the manuscript.

References

Anderson, R.C., Weiler, E.J.: 1978, *Astrophys. J.* **224**, 143
Baliunas, S.L., Guinan, E.F., Dupree, A.K.: 1984, *Astrophys. J.* **282**, 733
Bevington, P.R.: 1969, *Data Reduction and Error Analysis for the Physical Sciences*, McGraw, New York
Bohlin, R.C.: 1986, *Astrophys. J.* **308**, 1001
Bohlin, R.C., Grillmair, C.J.: 1987, *IUE NASA Newsletter*, **33**, 28
Bopp, B.W.: 1981, *Astron. J.* **86**, 771
Bopp, B.W.: 1983, in *Activity in Red Dwarf Stars*, *IAU Colloq. 71*, eds. P.B. Byrne, M. Rodonò, Reidel, Dordrecht, p. 363
Bornmann, P.L.: 1987, *Astrophys. J.* **313**, 449
Brown, A., Ferraz, M.C. de M., Jordan, C.: 1984, *Monthly Notices Roy. Astron. Soc.* **207**, 831
Brown, A., Jordan, C.: 1981, *Monthly Notices Roy. Astron. Soc.* **196**, 757
Brown, R.L., Crane, P.C.: 1978, *Astron. J.* **83**, 1504
Bruner, M.E., McWhirter, R.W.P.: 1988, *Astrophys. J.* **326**, 1002
Buzasi, D.L., Ramsey, L.W., Huenemoerder, D.P.: 1987, *Astrophys. J.* **322**, 353
Byrne, P.B., Doyle, J.G., Brown, A., Linsky, J.L., Rodonò, M.: 1987, *Astron. Astrophys.* **180**, 172 (Paper VI)
Canfield, R.C., et al.: 1980, in *Solar Flares*, ed. P.A. Sturrock, Colorado Associated University Press, p. 451
Catalano, S.: 1986, in Rutherford Appleton Laboratory Workshop on Astronomy and Astrophysics, *Flares: Solar and Stellar*, p. 105
Doyle, J.G., Kingston, A.E., Reid, R.H.G.: 1980, *Astron. Astrophys.* **90**, 97
Dulk, G.A.: 1985, *Ann. Rev. Astron. Astrophys.* **23**, 169
Fekel, F.C.: 1983, *Astrophys. J.* **268**, 274
Feldman, P.A.: 1980, in *Close Binary Stars: Observations and Interpretations*, eds. M.J. Plavec, D.M. Popper, R.K. Ulrich, Reidel, Dordrecht, p. 403
Feldman, P.A.: 1983, in *Activity in Red Dwarf Stars*, *IAU Colloq.* **71**, eds. P.B. Byrne, M. Rodonò, Reidel, Dordrecht, p. 429
Fraquelli, D.: 1982, *Astrophys. J. Letters* **254**, L41
Fraquelli, D.: 1984, *Astrophys. J.* **276**, 243
Furenlid, I., Young, A.: 1978, *Astron. J.* **83**, 1527
Gibson, D.M.: 1980, in *Close Binary Stars: Observations and Interpretations*, *IAU Colloq.* **88**, eds. M.J. Plavec, D.M. Popper, R.K. Ulrich, Reidel, Dordrecht, p. 405
Gibson, D.M.: 1981, in *Solar Phenomena in Stars and Stellar Systems*, eds. R.M. Bonnet, A.K. Dupree, Reidel, Dordrecht, p. 545
Hall, D.S.: 1976, in *Multiple Periodic Variable Stars*, *IAU Colloq.* **29**, ed. W.S. Fitch, Reidel, Dordrecht, p. 287
Hjellming, R.M., Gibson, D.M.: 1980, in *Radio Physics of the Sun*, *IAU Symp.* **86**, eds. M.R. Kundu, T.E. Gergely, Reidel, Dordrecht, p. 209
Keenan, F.P., Dufton, P.L., Kingston, A.E.: 1987, *Monthly Notices Roy. Astron. Soc.* **225**, 859
Lestrade, J.-F., Mutel, R.L., Phillips, R.B., Webber, J.C., Niell, A.E., Preston, R.A.: 1984, *Astrophys. J. Letters* **282**, L23
Linsky, J.L.: 1983, in *Cool Stars, Stellar Systems, and the Sun*, eds. S.L. Baliunas, L. Hartmann, Springer, Berlin, Heidelberg, New York, p. 244
Linsky, J.L., Neff, J.E., Gross, B.D., Simon, T., Andrews, A.D., Rodonò, M.: 1986, in *New Insights in Astrophysics*, ESA SP-**263**, p. 161
Machado, M.E., Avrett, E.H., Vernazza, J.E. Noyes, R.W.: 1980, *Astrophys. J.* **242**, 336
McWhirter, R.W.P., Thonemann, P.C., Wilson, R.: 1975, *Astron. Astrophys.* **40**, 63
Mullan, D.J.: 1985, in *Radio Stars*, eds. R.M. Hjellming, D.M. Gibson, Reidel, Dordrecht, p. 173
Murthy, J., Henry, R.C., Moos, H.W., Landsman, W.B., Linsky, J.L., Vidal-Madjar, A., Gry, C.: 1987, *Astrophys. J.* **315**, 675
Mutel, R.L., Lestrade, J.F., Preston, R.A., Phillips, R.B.: 1985, *Astrophys. J.* **289**, 262
Neff, J.E.: 1987, unpublished Ph.D. thesis, University of Colorado
Owen, F.N., Jones, T.W., Gibson, D.M.: 1976, *Astrophys. J. Letters* **210**, L27
Patkos, L.: 1981, *Astrophys. Letters* **22**, 1
Raymond, J.C., Cox, D.P., Smith, B.W.: 1976, *Astrophys. J.* **204**, 290.
Rodonò, M.: 1983, *Adv. Space Res.* **2**, No. 9, 225
Rodonò, M., et al.: 1986, *Astron. Astrophys.* **165**, 135 (Paper I)
Rodonò, M., Byrne, P.B., Neff, J.E., Linsky, J.L., Simon, T., Butler, C.J., Catalano, S., Cutispoto, G., Doyle, J.G., Andrews, A.D., Gibson, D.M. 1987, *Astron. Astrophys.* **176**, 267 (Paper III)
Sarma, M.B.K., Ausekar, B.D., Rao, B.V.N.S.P., Oh, J.Y., Nha, I.-S.: 1985, *Publ. Astron. Soc. Japan* **37**, 107
Seaton, M.J.: 1962, *Proc. Phys. Soc. London* **79**, 1105
Simon, T., Linsky, J.L., Schiffer, F.H. III: 1980, *Astrophys. J.* **239**, 911
Simon, T., Sonneborn, G.: 1987, *Astron. J.* **94**, 1657
Uchida, Y., Sakurai, T.: 1983, in *Activity in Red Dwarf Stars*, *IAU Coll.* **71**, eds. P.B. Byrne, M. Rodonò, Reidel, Dordrecht, p. 411
Vogt, S.S., Penrod, G.D.: 1983, *Publ. Astron. Soc. Pacific* **95**, 565
Walter, F.M., Brown, A., Linsky, J.L., Rydgren, E., Vrba, F., Roth, M., Carrasco, L., Chugainov, P.F., Shakovskaya, N.I., Imhoff, C.L.: 1987a, *Astrophys. J.* **314**, 297
Walter, F.M., Neff, J.E., Gibson, D.M., Linsky, J.L., Rodonò, M., Gary, D.E., Butler, C.J.: 1987b, *Astron. Astrophys.* **186**, 241 (Paper IV)
Weiler, E.J., et al.: 1978, *Astrophys. J.* **225**, 919